

# Symmetry-Induced Selective Excitation of Topological States in Su–Schrieffer–Heeger Waveguide Arrays

Min Tang,\* Jiawei Wang, Sreeramulu Valligatla, Christian N. Saggau, Haiyun Dong, Ehsan Saei Ghareh Naz, Sebastian Klembt, Ching Hua Lee, Ronny Thomale, Jeroen van den Brink, Ion Cosma Fulga,\* Oliver G. Schmidt, and Libo Ma

The investigation of topological state transition in carefully designed photonic lattices is of high interest for fundamental research, as well as for applied studies such as manipulating light flow in on-chip photonic systems. Herein, the topological phase transition between symmetric topological zero modes (TZM) and antisymmetric TZMs in Su–Schrieffer–Heeger mirror symmetric waveguides is reported. The transition of TZMs is realized by adjusting the coupling ratio between neighboring waveguide pairs, which is enabled by selective modulation of the refractive index in the waveguide gaps. Bidirectional topological transitions between symmetric and antisymmetric TZMs can be achieved with proposed switching strategy. Selective excitation of topological edge mode is demonstrated owing to the symmetry characteristics of the TZMs. The flexible manipulation of topological states is promising for on-chip light flow control and may spark further investigations on symmetric/antisymmetric TZM transitions in other photonic topological frameworks.

photonic lattices.<sup>[5]</sup> Introducing topology into photonics brings unprecedented properties such as topologically protected transport<sup>[6]</sup> or optical isolation,<sup>[7]</sup> which has become an intensely investigated field of research. Photonic topological states play a unique role in molding the flow of light,<sup>[8]</sup> lasing,<sup>[9]</sup> non-Hermitian photonics,<sup>[10]</sup> and nonlinear optics.<sup>[11]</sup> Quasicrystals can also exhibit nontrivial topological properties. The topological nature of these states is utilized to adiabatically pump light across the quasicrystals.<sup>[12]</sup> The implementation of transitions was achieved by femtosecond laser writing in bulk glass<sup>[12b]</sup> circuit board printing<sup>[12a]</sup> which supports optical modes in the telecom spectral range and surface plasmon polariton modes, respectively. Topological photonic devices with switchable phase transitions are of high interest

## 1. Introduction

Topological insulators represent a new class of materials that have a bulk bandgap like an ordinary insulator, while exhibiting gapless topological edge or surface states.<sup>[1]</sup> Topological insulators have been realized in various physical systems that can be characterized by wave equations, including condensed matter systems,<sup>[2]</sup> acoustic systems,<sup>[3]</sup> electric circuits,<sup>[4]</sup> and

not only for fundamental studies in controlling lightwave flow with the desired frequency, polarization, and propagating direction but also for practical applications including optical modulation, filters, and on-chip quantum computing.

However, in previous reports, the photonic devices are usually rigid against switching of the topological properties. To investigate topological phase transition, some pioneering works have been reported.<sup>[13]</sup> For example, spatially structured laser

M. Tang, J. Wang, S. Valligatla, C. N. Saggau, H. Dong, E. Saei Ghareh Naz, L. Ma  
Institute for Integrative Nanosciences  
Leibniz Institute for Solid State and Materials Research  
01069 Dresden, Germany  
E-mail: m.tang@ifw-dresden.de

J. Wang  
School of Electronic and Information Engineering  
Harbin Institute of Technology (Shenzhen)  
Shenzhen 518055, China

 The ORCID identification number(s) for the author(s) of this article can be found under <https://doi.org/10.1002/adpr.202300113>.

© 2023 The Authors. Advanced Photonics Research published by Wiley-VCH GmbH. This is an open access article under the terms of the Creative Commons Attribution License, which permits use, distribution and reproduction in any medium, provided the original work is properly cited.

DOI: 10.1002/adpr.202300113

S. Klembt  
Technische Physik  
Wilhelm-Conrad-Röntgen-Research Center for Complex Material Systems, and Würzburg–Dresden Cluster of Excellence ct.qmat  
Universität Würzburg  
D-97074 Würzburg, Germany

C. H. Lee  
Department of Physics  
National University of Singapore  
Singapore 117551, Singapore

R. Thomale  
Institute for Theoretical Physics and Astrophysics  
University of Würzburg  
D-97074 Würzburg, Germany

J. van den Brink, I. C. Fulga  
Institute for Theoretical Solid State Physics  
Leibniz Institute for Solid State and Materials Research  
01069 Dresden, Germany  
E-mail: i.c.fulga@ifw-dresden.de

excitations have been utilized to reconfigure non-Hermitian junctions for the control of topological interface states.<sup>[13d]</sup> By changing polarization states, distinct topological phases and polariton edge states were obtained in perovskite lattices.<sup>[13c]</sup> Moreover, topological edge mode switching can also be realized by thermal-induced insulator-to-metal transition.<sup>[13a]</sup> Despite these advances, it is highly demanded to explore and demonstrate novel switching strategies that can realize a transition between different topological states for selective excitation of nontrivial/trivial states.

Here, we design and fabricate reconfigurable one-dimensional (1D) photonic topological insulators composed of SiN<sub>x</sub> waveguide arrays for the demonstration of topological state switching. Drawing on an earlier theoretical proposal,<sup>[14]</sup> the photonic device is based on a Su–Schrieffer–Heeger (SSH) model<sup>[15]</sup> where the coupling strengths (denoted  $\kappa_1$  and  $\kappa_2$ ) can be varied between adjacent waveguide pairs. As shown in Figure 1a,b, the dimerized coupling is realized by alternately filling the interwaveguide gaps with polymethyl methacrylate (PMMA). The waveguide arrays are designed to be symmetrically distributed at the two sides of a center waveguide (see Figure 1c) which serves as the light input. With this symmetric design, depending on the dimerization ( $\kappa_1 > \kappa_2$  or  $\kappa_1 < \kappa_2$ ), either a symmetric TZMs or an antisymmetric TZMs is localized at the central waveguide. For the plasmonic waveguide array with a kinked structure, the nonspreading interface mode can be excited in the realistic excitation of single waveguide input.<sup>[16]</sup> To enable a phase transition between symmetric and antisymmetric TZMs, the air gaps can be filled by ethanol (EtOH) solution (see Figure 1d), which increases the coupling strength therein and in turn enables an inversion of the coupling strength ratio ( $\kappa_1/\kappa_2$ ). Alternatively, the topological phase transition can also be obtained by modifying the PMMA through electron beam irradiation (EBI) which can change the coupling strength at the PMMA-filled gaps (Figure 1d). It should be noted that the gap width is designed to be different to match the coupling strength difference in Figure 1d. With these methods, bidirectional transitions between the symmetric and antisymmetric TZMs are realized in arrays A and B. Our work presents the switching of the topological phases, which paves the way for the switching of topological states of

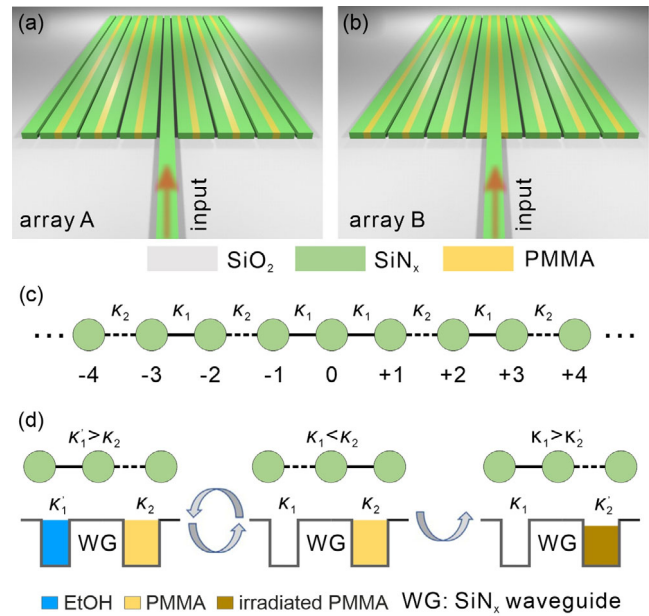


**Figure 1.** Schematic diagram of switchable topological SiN<sub>x</sub> waveguide arrays with mirror symmetry at a central waveguide. For a) array A and b) array B, the gaps from the central waveguide to the side waveguides are periodically filled by air-PMMA-air and PMMA-air-PMMA, respectively. c) Schematic of the system with an alternating coupling between neighboring waveguides. In this example, the solid and dashed lines indicate strong and weak coupling, respectively, such that  $\kappa_1 > \kappa_2$ . d) Coupling strength inversion enabled by filling the air gaps with ethanol solution (left panel) or modifying the PMMA (right panel) by electron beam irradiation.

light to control the light flow in on-chip integrated topological photonic devices.

## 2. Results and Discussion

The system can be described based on coupled-mode theory (CMT),<sup>[17]</sup> which reveals the spatial evolution of optical modes, as well as the eigenmode characteristics. In the present one-dimensional symmetrically-coupled system of  $2N + 1$  waveguides,  $j$  enumerates the waveguides, where the  $j^{\text{th}}$  waveguide ( $j = 0, \pm 1, \dots, \pm N$ ) indicates its relative position to the central waveguide. Each single waveguide has identical geometrical parameters with the same propagation constant  $\beta_0$ . The coupling strengths from the central to peripheral waveguides are  $\kappa_1$  and  $\kappa_2$  with periodic alternation. The amplitude  $a_j(z)$  of the central and peripheral optical modes evolves along the propagating direction as

$$i \frac{\partial a_0(z)}{\partial z} + \beta_0 a_0(z) + \kappa_1 (a_{+1}(z) + a_{-1}(z)) = 0 \quad (1)$$

$$i \frac{\partial a_j(z)}{\partial z} + \beta_0 a_j(z) + \kappa_1 a_{j+\text{sign}(j)}(z) + \kappa_2 a_{j-\text{sign}(j)}(z) = 0 \quad (\text{for } \text{mod}(|j|, 2) = 0) \quad (2)$$

J. van den Brink  
Institut für Theoretische Physik and Würzburg–Dresden Cluster of Excellence ct.qmat  
Technische Universität Dresden  
01062 Dresden, Germany

O. G. Schmidt  
Research Center for Materials, Architectures and Integration of Nanomembranes (MAIN)  
Technische Universität Chemnitz  
D-09126 Chemnitz, Germany

O. G. Schmidt  
Material Systems for Nanoelectronics  
Chemnitz University of Technology  
D-09111 Chemnitz, Germany

O. G. Schmidt  
Nanophysics  
Dresden University of Technology  
D-01069 Dresden, Germany

$$i \frac{\partial a_j(z)}{\partial z} + \beta_0 a_j(z) + \kappa_2 a_{j+\text{sign}(j)}(z) + \kappa_1 a_{j-\text{sign}(j)}(z) = 0 \text{ (for } \text{mod}(|j|, 2) = 1) \quad (3)$$

The  $a_{j+\text{sign}(j)}(z)$  terms for the edges of the waveguide array in Equation (2) and (3) can be discarded because of the open boundary conditions. This treatment is completely analogous to the tight-binding Hamiltonian model in condensed matter physics, where evolving in  $z$  direction is an analog to time.<sup>[18]</sup> Away from the central waveguide, the bulk Hamiltonian takes the same form as the SSH model discussed in a previous report,<sup>[19]</sup> which implies a similar topological behavior of the TZMs supported by the edge waveguides. For an infinite SSH lattice, the Hamiltonian can be expressed in momentum space as

$$H(k) = \begin{pmatrix} 0 & \rho^*(k) \\ \rho(k) & 0 \end{pmatrix} \quad (4)$$

where  $\rho(k) = \kappa_1 + \kappa_2 e^{ik}$ . The Hamiltonian exhibits two distinct states depending on the two possible situations of  $\kappa_1 > \kappa_2$  and  $\kappa_1 < \kappa_2$ , corresponding to trivial and nontrivial topological phases, respectively.<sup>[20]</sup> The winding number as well as the Zak phase in the Brillouin zone is determined by the  $\kappa_1/\kappa_2$  ratio and can be calculated via  $\oint \langle dk u_k | \partial_k u_k \rangle$ .<sup>[21]</sup> The Zak phase  $Z$  yields  $Z = 0/\pi$  in the case of  $\kappa_1 > \kappa_2/\kappa_1 < \kappa_2$ , respectively. A nonzero winding number or Zak phase implies nontrivial topology and thus indicates the existence of topological edge states.

It should be noted that for both dimerizations ( $\kappa_1 > \kappa_2$  and  $\kappa_1 < \kappa_2$ ), a TZM is present around the central waveguide in our design. This is because the central waveguide represents a defect across which the dimerization pattern changes. The central TZM, however, is either antisymmetric or symmetric to the central waveguide in real space, corresponding to the case of  $\kappa_1 > \kappa_2$  or  $\kappa_1 < \kappa_2$ . For the case of the symmetric TZM, the maximum optical field is located at the central waveguide, where the optical field distribution can be folded symmetrically ( $a_j(z) = a_{-j}(z)$ ). For the antisymmetric TZM, there exists  $a_0(z) = 0$  at the central waveguide and  $a_j(z) = -a_{-j}(z)$  for the symmetrically distributed waveguide pairs. As such, symmetric and antisymmetric TZMs with different optical field distributions can be manipulated by changing  $\kappa_1/\kappa_2$  in the waveguide arrays.

In the fabricated waveguide array with open boundaries,  $2N + 1 = 59$  waveguides are designed. **Figure 2a,c** shows the results calculated based on the Hamiltonian with open boundary condition, where the bulk bandgap opens for both  $\kappa_1 > \kappa_2$  and  $\kappa_1 < \kappa_2$ , supporting different types of TZM. For the case of  $\kappa_1 > \kappa_2$ , a TZM only occurs at the central part (i.e., waveguides next to the central one) of the waveguide array with an antisymmetric distribution, while a symmetric TZM is present at the central waveguide together with two additional TZMs located at the two sides of the waveguide array for the case of  $\kappa_1 < \kappa_2$ , as shown in **Figure 2b,d**. In the design of input through the central waveguide, the symmetry of the TZM at the central waveguide determines the excitation efficiency of the corresponding states (i.e., the symmetric and antisymmetric TZMs) in the waveguide array. The overlap ratio between the central waveguide and the eigenstate was calculated to be 0.59 for the

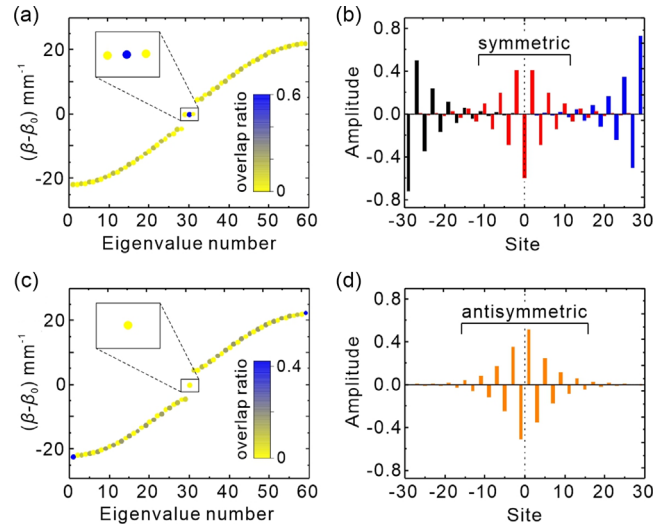


**Figure 2.** The calculated spectrum of the SSH waveguide arrays consisting of 59 waveguides with mirror symmetry to a central waveguide, obtained by solving for the eigenvalues of open boundary Hamiltonian with a)  $\kappa_1 = 9 \text{ mm}^{-1}$ ,  $\kappa_2 = 13 \text{ mm}^{-1}$ , and c)  $\kappa_1 = 13 \text{ mm}^{-1}$ ,  $\kappa_2 = 9 \text{ mm}^{-1}$ . The overlap ratios in (a) and (c) characterize the overlap between the eigenmode and the central waveguide. b) Real-space distributions of the TZMs at the edge sites (blue and black) and the symmetric TZM at the center waveguide (red, site = 0) corresponding to the case of (a). d) Real-space distribution of the antisymmetric TZM corresponding to the case of (c).

symmetric TZM, as shown in **Figure 2a**, while the antisymmetric TZM has a zero overlap, as shown in **Figure 2c**. In other words, the TZM can be efficiently excited via the central waveguide when  $\kappa_1 < \kappa_2$ , while only trivial bulk states can be excited when  $\kappa_1 > \kappa_2$ .

Based on the above theoretical analysis, we fabricated  $\text{SiN}_x$  waveguide arrays for the demonstration of topological phase transition by changing the  $\kappa_1/\kappa_2$  ratio. Each element of the waveguide array, including the center one, is a  $\text{SiN}_x$  waveguide with a refractive index  $n = 2.02$  (@836 nm). The width, height, and length of the  $\text{SiN}_x$  waveguides are  $1.5 \mu\text{m}$ ,  $200 \text{ nm}$ , and  $500 \mu\text{m}$ , respectively. The waveguide arrays are prepared on a Si substrate spaced by a  $2 \mu\text{m}$  thick  $\text{SiO}_2$  layer. The  $\text{SiO}_2$  layer has a refractive index of 1.45, which prevents optical leakage to the substrate. The coupling behavior in a pair of waveguides was examined by the beam propagating method (**Figure 3**) in a 3D configuration (Comsol Multiphysics 5.3). Gap-1 and 2 in **Figure 1** are designed as 120 and 220 nm in width which are filled by air and PMMA, respectively. The inversion of the coupling ratio  $\kappa_1/\kappa_2$  is realized by either increasing the coupling strength  $\kappa_1$  at the hollow gap-1 or decreasing  $\kappa_2$  at gap-2. The increase of  $\kappa_1$  can be obtained by filling the hollow gap-1 with EtOH solution (refractive index of 1.36), by which the refractive index of gap-1 can significantly increase while that of gap-2 is constant. The decrease of  $\kappa_2$  at gap-2 can be achieved by irradiating the filled PMMA using an electron beam (5 keV,  $0.02 \mu\text{C cm}^{-2}$ , 3 min 25 s) in a scanning electron microscope (DSM982, Carl Zeiss Microscopy GmbH) while the  $\kappa_1$  at gap-1 is intact during this process. The high-energy electrons can break chemical bonds and significantly

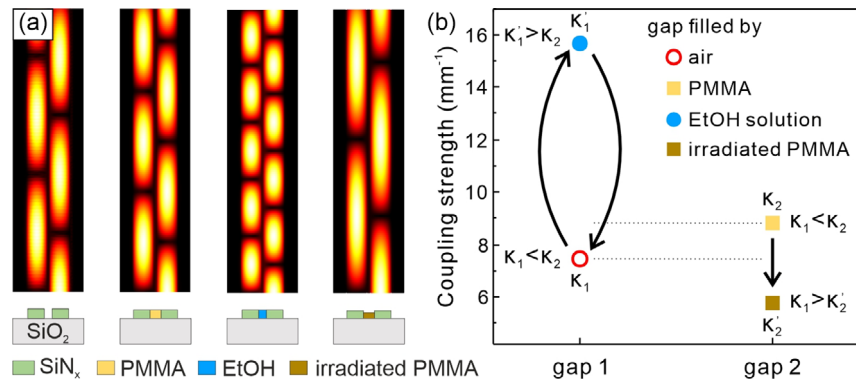


**Figure 3.** a) Simulated optical field ( $|H_z|$ ) distributions under the coupling of fundamental modes propagating along a pair of neighboring waveguides. The gaps of the waveguides are filled by air, PMMA, EtOH solution, and electron-irradiation-modified PMMA. b) The corresponding coupling strength between the waveguides for the four situations.

change the chemical composition of the filled PMMA.<sup>[22]</sup> This process generates several effects on the PMMA, including decreasing the refractive index in the near-infrared range,<sup>[23]</sup> thinning the membrane,<sup>[24]</sup> and introducing roughness at its surface,<sup>[22]</sup> all of which will reduce the coupling strength at gap-2. In the simulation, a reduction of 0.1 of the refractive index and 50 nm of the PMMA thickness is considered. The mode distributions of four coupling situations are presented in Figure 3a, corresponding to a gap filled by air, PMMA, EtOH solution, and irradiated PMMA, respectively. The corresponding coupling strength variations from  $\kappa$  to  $\kappa'$  are presented in Figure 3b, showing the capability of inverting the coupling ratio  $\kappa_1/\kappa_2$ . The experiment setup and SEM images are shown in **Figure 4**. More details can be found in the experimental section.

Based on the analysis in Figure 2, manipulating the coupling ratio in the SSH lattice can change the symmetry and distribution of the TZM at the central waveguide, which results in its selective excitation. When the system supports a symmetric TZM ( $\kappa_1 < \kappa_2$ ), it can be effectively excited through the central waveguide, as it has a maximum field distribution therein. For the case of an antisymmetric TZM, only bulk states (rather than topological states within the bandgap) can be excited through the central waveguide, as it has a zero distribution of the TZM at the central waveguide. In the experimental verification, the field distribution at the end of the waveguide array is examined to distinguish bulk and in-gap modes excited through the central waveguide. In the air background, the design of array-A and array-B satisfies  $\kappa_1 < \kappa_2$  and  $\kappa_1 > \kappa_2$ , respectively. Hence, array-A/array-B supports a symmetric/antisymmetric TZM, which has a large/zero overlap with the initial state. The bulk modes can also be excited when  $\kappa_1 < \kappa_2$  due to the fact that the eigenstate was not used as the initial state to excite the system. Nevertheless, most energy will be transferred into the symmetric TZM and a center peak emerges when being excited through the center waveguide. When  $\kappa_1 > \kappa_2$ , only bulk modes can be excited and a broadened scattering light at the end facets of the waveguide array is observed. In the deposition and etching process, impurity and the rough edge can be introduced to the waveguides. In **Figure 5b,e**, the samples were filled with the EtOH solution, which causes a different distribution of

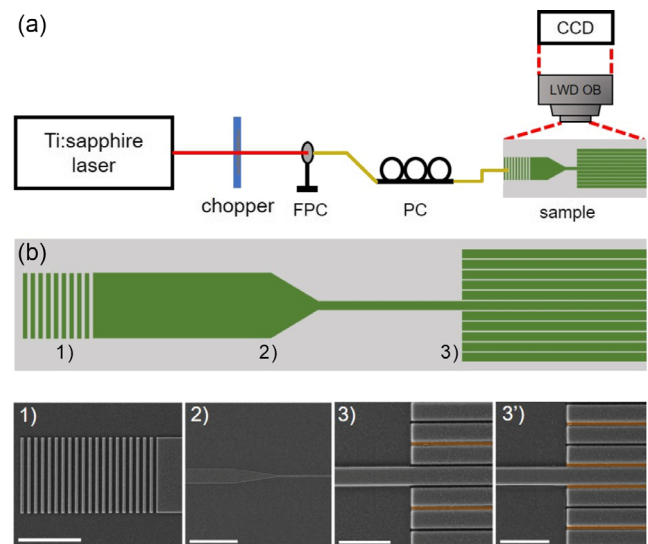


**Figure 4.** a) Schematic diagram of the optical characterization setup. FPC, fiber port coupler; PC, polarization controller; LWDOB, long-working-distance objective lens. The red solid line represents the optic path in free space. The yellow lines represent light guided through an optical fiber. b) Schematic diagram and SEM images corresponding to different parts of the waveguide array consisting of 1) grating coupler, 2) waveguide mode converter, 3) waveguide array A, and 3') waveguide array B. The corresponding scale bars are 10, 40, 4, and 4  $\mu\text{m}$ , respectively. The yellow regions in 3) and 3') indicate the gaps filled by PMMA.

the refractive index in the vertical direction. Compared to the case of air, the refractive index of EtOH solution is closer to the substrate, so the light has a larger probability to couple to the upward loss channel as the refractive contrast of EtOH/ $\text{SiN}_x$  is smaller than Air/ $\text{SiN}_x$ . In Figure 5c, the irradiation of the electron beam can cause an increase in surface defects and also lead to an increased upward leakage. Topological phase transitions were observed in array A by either filling with 90% EtOH solution or EBI. These processes enable a transition from a symmetric TZM, which can be excited through the central waveguide (see Figure 5a), to an antisymmetric TZM where only trivial bulk modes can be excited through the central waveguide

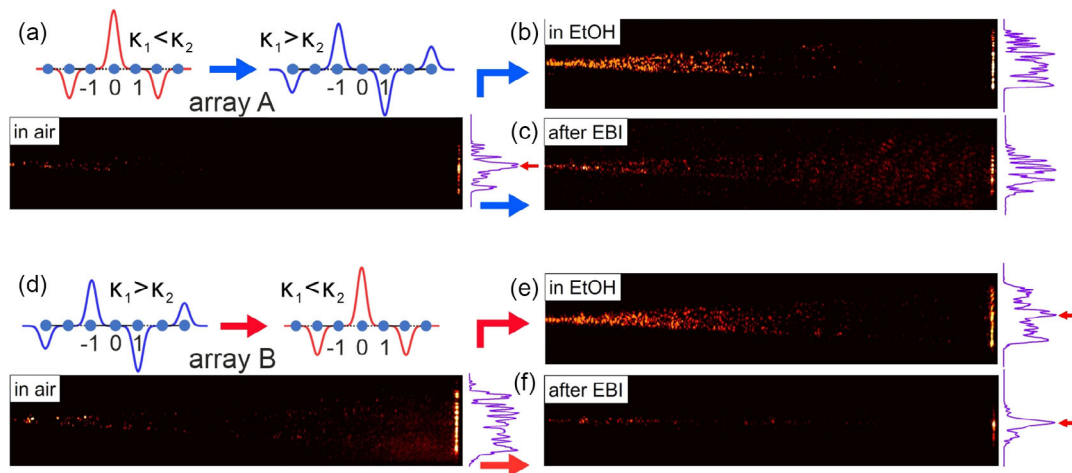


**Figure 5.** Measurement results of the optical transport characteristics in the waveguide array A and B. Panels a–c) show a symmetric to antisymmetric transition of the TZM in waveguide array A, which can be seen from mode field distributions along the waveguides and corresponding field intensity distributions at the end facets of waveguide array. Panels d–f) show the antisymmetric to symmetric transition of the TZM with corresponding field and intensity distributions in the waveguide array B. For (a) and (d), the sample is in air, while for (b) and (e), the samples are filled with 90% EtOH solution. For (c) and (f), the sample is measured after EBI. The height of the image is exactly the same as the waveguide array region while the width of the images is slightly larger than the waveguide length to present the scattering field at the end facets. The schematic only shows the central waveguide site and its nearest sites.

(Figure 5b,c). As shown in Figure 5a, a localized mode was observed at the central waveguide of array A, which is designed to have  $\kappa_1 < \kappa_2$ . After filling with 90% EtOH solution or EBI, the coupling strength is changed to be  $\kappa_1 > \kappa_2$ , where the system supports an antisymmetric TZM. As such, the previously observed TZM disappeared, while only bulk modes can be excited through the central waveguide (Figure 5b,c). A reverse transition from antisymmetric to symmetric TZMs is also realized in array B by the same processing methods, as shown in Figure 5d–f. Waveguide array B was designed with  $\kappa_1 > \kappa_2$ , supporting an antisymmetric TZM that cannot be excited efficiently through the central waveguide. The coupling ratio was inverted to be  $\kappa_1 < \kappa_2$  to support a symmetric TZM after filling with 90% EtOH solution or EBI processing. As a result, the topological mode can be excited and observed at the central waveguide (Figure 5e,f). For the case of  $\kappa_1 > \kappa_2$ , a trivial defect state (TDS) which is known as the Tamm state can appear relying on the strong-weak coupling configured at the kinked defect waveguide to the neighboring waveguides.<sup>[15a,d]</sup> For the case of  $\kappa_1 < \kappa_2$  which supports the symmetric TZM, TDS is not supported due to the weak–strong coupling configuration at the defect region. The localized modes observed in Figure 5a,e,f can only be caused by the excitation of the TZM. For the case of  $\kappa_1 > \kappa_2$  which in principle can support the antisymmetric TZM and TDS simultaneously, while in our measurement only broadening scattered light at the end facets is observed from Figure 5b–d due to the following two reasons: 1) The antisymmetric TZM is not excited due to the zero overlap with the initial state; 2) The TDS is not strongly localized due to the low coupling strength contrast at the defect region.<sup>[15a,d]</sup> The chemical component change of PMMA is not reversible after electron beam irradiation, however, introducing a switchable material such as organic fluorescent dye controlled through UV/visible photoirradiation<sup>[25]</sup> could be a potential solution for realizing a reversible

topological phase transition by controlling the gap-filling material.

### 3. Conclusion

In summary, topological transitions between symmetric and antisymmetric TZMs have been theoretically and experimentally demonstrated in SSH waveguide arrays designed with mirror symmetry. The transition of TZMs is enabled by manipulating the coupling ratio between neighboring waveguide pairs via liquid filling or electron beam irradiation. Due to the symmetry characteristics of the TZM, either the topological mode or trivial bulk modes can be selectively excited through a central waveguide in the SSH arrays. Our work enables the reshaping of TZMs in the center region of 1D systems for the manipulation and switch of topological states. Moreover, this work is promising for extending to other topological systems, such as the higher-dimensional SSH lattices where the antisymmetric/symmetric TZMs can potentially be designed in multiple directions,<sup>[26]</sup> non-Hermitian topological photonic systems providing bulk-boundary correspondence,<sup>[27]</sup> and nonlinear topological systems with nonlinearity-induced topological phase transitions.<sup>[11a,28]</sup>

### 4. Topological Phase Transition Analysis

In the following, we will show that the transition from a symmetric to an antisymmetric TZM in a mirror-symmetric SSH chain is a topological phase transition, i.e., it cannot occur without closing and reopening of the bulk gap.

Consider a mirror-symmetric SSH chain that consists of  $2N + 1$  sites and contains a defect in the middle (position  $x = 0$ ), as shown in Figure 1c. The Hamiltonian of the system obeys a chiral



The sample consists of 1) grating coupler, 2) mode converter, and 3) waveguide arrays. The width and grating period of the grating coupler are 12.0 and 1.0  $\mu\text{m}$ , respectively. Considering the phase-matching condition, the injection fiber angle will be adjusted when the sample is in the air/EtOH solution background. In the measurement setup, a wavelength-tunable Ti:sapphire laser at 836 nm is end-fired into the grating coupler assisted by an optical chopper, fiber-port coupler, and polarization controller. The sample is mounted in a Petri dish which is convenient for solution filling. To image light-scattering patterns from the top view of the waveguide arrays, a long-working-distance microscope objective lens (37 mm) is used together with an 8 MP monochrome CCD camera (S805MU2).

## Acknowledgements

This work was financially supported by the Würzburg-Dresden Cluster of Excellence on Complexity and Topology in Quantum Matter—ct.qmat (EXC 2147, project-ID 390858490). L.B.M. acknowledges financial support by the German Research Foundation (MA 7968/2-1). J. W. acknowledges the support of the National Natural Science Foundation of China (grant no. 62105080) and the Program for International S&T Cooperation Projects of Guangdong Province (grant no. 2022A0505030003). O.G.S. acknowledges financial support from the Leibniz Program of the German Research Foundation (SCHM 1298/26-1). The authors thank M. Bauer, L. Raith, and R. Engelhard for the technical support; S. Baunack for helpful discussion and SEM characterizations.

Open Access funding enabled and organized by Projekt DEAL.

## Conflict of Interest

The authors declare no conflict of interest.

## Data Availability Statement

The data that support the findings of this study are available from the corresponding author upon reasonable request.

## Keywords

optical waveguides, phase transition, topological photonics

Received: April 3, 2023

Revised: August 23, 2023

Published online: September 10, 2023

- [1] M. Z. Hasan, C. L. Kane, *Rev. Mod. Phys.* **2010**, *82*, 3045.  
 [2] a) N. H. Lindner, G. Refael, V. Galitski, *Nat. Phys.* **2011**, *7*, 490; b) B. Yan, L. Muehler, C. Felser, *Phys. Rev. Lett.* **2012**, *109*, 116406; c) E. J. Meier, F. A. An, B. Gadway, *Nat. Commun.* **2016**, *7*, 13986.  
 [3] a) C. He, X. Ni, H. Ge, X.-C. Sun, Y.-B. Chen, M.-H. Lu, X.-P. Liu, Y.-F. Chen, *Nat. Phys.* **2016**, *12*, 1124; b) Z. Yang, F. Gao, X. Shi, X. Lin, Z. Gao, Y. Chong, B. Zhang, *Phys. Rev. Lett.* **2015**, *114*, 114301.  
 [4] a) V. V. Albert, L. I. Glazman, L. Jiang, *Phys. Rev. Lett.* **2015**, *114*, 173902; b) S. Imhof, C. Berger, F. Bayer, J. Brehm, L. W. Molenkamp, T. Kiessling, F. Schindler, C. H. Lee, M. Greiter, T. Neupert, *Nat. Phys.* **2018**, *14*, 925; c) A. Stegmaier, S. Imhof, T. Helbig, T. Hofmann, C. H. Lee, M. Kremer, A. Fritzsche, T. Feichtner, S. Klembt, S. Höfling, *Phys. Rev. Lett.* **2021**, *126*, 215302.  
 [5] a) W. Hu, J. C. Pillay, K. Wu, M. Pasek, P. P. Shum, Y. Chong, *Phys. Rev. X* **2015**, *5*, 011012; b) A. B. Khanikaev, G. Shvets, *Nat. Photonics* **2017**, *11*, 763; c) Z. Wang, Y. Chong, J. D. Joannopoulos, M. Soljačić, *Nature* **2009**, *461*, 772.  
 [6] M. Hafezi, E. A. Demler, M. D. Lukin, J. M. Taylor, *Nat. Phys.* **2011**, *7*, 907.  
 [7] K. Fang, Z. Yu, S. Fan, *Nat. Photonics* **2012**, *6*, 782.  
 [8] a) J. D. Joannopoulos, S. G. Johnson, J. N. Winn, R. D. Meade, Princeton University Press, Princeton, NJ **2008**; b) L. Lu, J. D. Joannopoulos, M. Soljačić, *Nat. Photonics* **2014**, *8*, 821.  
 [9] a) M. A. Bandres, S. Wittek, G. Harari, M. Parto, J. Ren, M. Segev, D. N. Christodoulides, M. Khajavikhan, *Science* **2018**, *359*, eaar4005; b) G. Harari, M. A. Bandres, Y. Lumer, M. C. Rechtsman, Y. D. Chong, M. Khajavikhan, D. N. Christodoulides, M. Segev, *Science* **2018**, *359*, eaar4003; c) Y. Zeng, U. Chattopadhyay, B. Zhu, B. Qiang, J. Li, Y. Jin, L. Li, A. G. Davies, E. H. Linfield, B. Zhang, *Nature* **2020**, *578*, 246.  
 [10] a) K. Wang, A. Dutt, C. C. Wojcik, S. Fan, *Nature* **2021**, *598*, 59; b) S. Yao, Z. Wang, *Phys. Rev. Lett.* **2018**, *121*, 086803.  
 [11] a) L. J. Maczewsky, M. Heinrich, M. Kremer, S. K. Ivanov, M. Ehrhardt, F. Martinez, Y. V. Kartashov, V. V. Konotop, L. Torner, D. Bauer, *Science* **2020**, *370*, 701; b) M. Guo, S. Xia, N. Wang, D. Song, Z. Chen, J. Yang, *Opt. Lett.* **2020**, *45*, 6466; c) S. Xia, D. Jukić, N. Wang, D. Smirnova, L. Smirnov, L. Tang, D. Song, A. Szameit, D. Leykam, J. Xu, *Light: Sci. Appl.* **2020**, *9*, 147.  
 [12] a) Q. Cheng, H. Wang, Y. Ke, T. Chen, Y. Yu, Y. S. Kivshar, C. Lee, Y. Pan, *Nat. Commun.* **2022**, *13*, 249; b) Y. E. Kraus, Y. Lahini, Z. Ringel, M. Verbin, O. Zilberberg, *Phys. Rev. Lett.* **2012**, *109*, 106402.  
 [13] a) C. Li, X. Hu, W. Gao, Y. Ao, S. Chu, H. Yang, Q. Gong, *Adv. Opt. Mater.* **2018**, *6*, 1701071; b) L. Li, C. H. Lee, J. Gong, *Phys. Rev. Lett.* **2020**, *124*, 250402; c) R. Su, S. Ghosh, T. C. Liew, Q. Xiong, *Sci. Adv.* **2021**, *7*, eabf8049; d) H. Zhao, X. Qiao, T. Wu, B. Midya, S. Longhi, L. Feng, *Science* **2019**, *365*, 1163.  
 [14] E. S. G. Naz, I. C. Fulga, L. Ma, O. G. Schmidt, J. van den Brink, *Phys. Rev. A* **2018**, *98*, 033830.  
 [15] a) A. Blanco-Redondo, I. Andonegui, M. J. Collins, G. Harari, Y. Lumer, M. C. Rechtsman, B. J. Eggleton, M. Segev, *Phys. Rev. Lett.* **2016**, *116*, 163901; b) A. Blanco-Redondo, B. Bell, D. Oren, B. J. Eggleton, M. Segev, *Science* **2018**, *362*, 568; c) W.-P. Su, J. R. Schrieffer, A. J. Heeger, *Phys. Rev. Lett.* **1979**, *42*, 1698; d) J. Wang, S. Xia, R. Wang, R. Ma, Y. Lu, X. Zhang, D. Song, Q. Wu, R. Morandotti, J. Xu, *Light: Sci. Appl.* **2022**, *11*, 152.  
 [16] Q. Cheng, Y. Pan, Q. Wang, T. Li, S. Zhu, *Laser Photonics Rev.* **2015**, *9*, 392.  
 [17] A. Block, C. Etrich, T. Limboeck, F. Bleckmann, E. Soergel, C. Rockstuhl, S. Linden, *Nat. Commun.* **2014**, *5*, 3843.  
 [18] D. Dunlap, V. Kenkre, *Phys. Rev. B* **1986**, *34*, 3625.  
 [19] P. St-Jean, V. Goblot, E. Galopin, A. Lemaître, T. Ozawa, L. Le Gratiet, I. Sagnes, J. Bloch, A. Amo, *Nat. Photonics* **2017**, *11*, 651.  
 [20] P. Delplace, D. Ullmo, G. Montambaux, *Phys. Rev. B* **2011**, *84*, 195452.  
 [21] D. Xiao, M.-C. Chang, Q. Niu, *Rev. Mod. Phys.* **2010**, *82*, 1959.  
 [22] R. Nathawat, A. Kumar, N. Acharya, Y. Vijay, *Surf. Coat. Technol.* **2009**, *203*, 2600.  
 [23] M. Rashidian, D. Dorrnanian, *J. Theor. Appl. Phys.* **2014**, *8*, 121.  
 [24] J. Yu, X. Tao, H. Tam, M. S. Demokan, *Appl. Surf. Sci.* **2005**, *252*, 1283.  
 [25] . Hendra, A. Takeuchi, H. Yamagishi, O. Oki, M. Morimoto, M. Irie, Y. Yamamoto, *Adv. Funct. Mater.* **2021**, *31*, 2103685.  
 [26] a) F. Liu, K. Wakabayashi, *Phys. Rev. Lett.* **2017**, *118*, 076803; b) B. Xing, W.-T. Chiu, D. Poletti, R. T. Scalettar, G. Batrouni, *Phys. Rev. Lett.* **2021**, *126*, 017601.  
 [27] a) M. Pan, H. Zhao, P. Miao, S. Longhi, L. Feng, *Nat. Commun.* **2018**, *9*, 1308; b) X. Zhu, H. Wang, S. K. Gupta, H. Zhang, B. Xie, M. Lu, Y. Chen, *Phys. Rev. Res.* **2020**, *2*, 013280.  
 [28] D. Leykam, Y. D. Chong, *Phys. Rev. Lett.* **2016**, *117*, 143901.